IEEE Photonics Journal
An IEEE Photonics Society Publication

Suppressing Dark Counts of Multimode-Fiber-Coupled Superconducting Nanowire Single-Photon Detector

Volume 11, Number 5, October 2019

Chengjun Zhang
Weijun Zhang
Lixing You
Jia Huang
Hao Li
Xingqu Sun
Heqing Wang
Chaolin Lv
Hui Zhou
Xiaoyu Liu
Zhen Wang
Xiaoming Xie

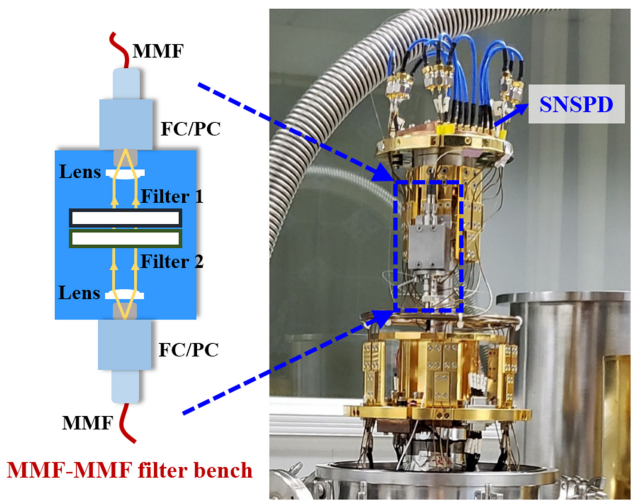

DOI: 10.1109/JPHOT.2019.2937537

Suppressing Dark Counts of Multimode-Fiber-Coupled Superconducting Nanowire Single-Photon Detector

Chengjun Zhang,[1,2,3] **Weijun Zhang**,[1,3] **Lixing You**,[1,2,3,4] **Jia Huang**,[1,2,3] **Hao Li**,[1,3] **Xingqu Sun**,[1,2,3] **Heqing Wang**,[1,2,3] **Chaolin Lv**,[1,3] **Hui Zhou**,[1,3] **Xiaoyu Liu**,[1,3] **Zhen Wang**,[1,3] **and Xiaoming Xie**[1,3]

[1]State Key Laboratory of Functional Materials for Informatics, Shanghai Institute of Microsystem and Information Technology, Chinese Academy of Sciences, Shanghai 200050, China
[2]Center of Materials Science and Optoelectronics Engineering, University of Chinese Academy of Sciences, Beijing 100049, China
[3]Center for Excellence in Superconducting Electronics, Chinese Academy of Sciences, Shanghai 200050, China
[4]Shanghai Photon Technology Company, Ltd., Shanghai 200050, China

DOI:10.1109/JPHOT.2019.2937537

Manuscript received June 26, 2019; revised August 1, 2019; accepted August 21, 2019. Date of publication August 26, 2019; date of current version September 6, 2019. This work was supported in part by the National Key R&D Program of China under Grant 2017YFA0304000, in part by the Science and Technology Commission of Shanghai Municipality under Grant 16JC1400402, and in part by the Program of Shanghai Academic/Technology Research Leader under Grant 18XD1404600. Corresponding author: Weijun Zhang (e-mail: zhangweijun@mail.sim.ac.cn).

Abstract: Large active-area superconducting nanowire single-photon detectors (SNSPDs) coupled with multimode fibers (MMFs) can provide high light-gathering capacity, which is essential for free-space detection applications in photon-starved regimes. However, MMF-coupled SNSPDs often suffer from large system dark count rates (DCR_{sys}) over kHz due to blackbody radiation of the MMF at room temperature. Such large DCR_{sys} would significantly degrade signal-to-noise ratio (SNR) of the receiving system. This paper reports an MMF-coupled large-active-area SNSPD system with low DCR_{sys} by using a homemade cryogenic MMF filter bench. The filter bench, which consists of lenses and optical filters, can provide a high transmittance of about 80% at the central wavelength of the passband (1550 ± 12.5 nm) and a wide blocking range from 500 nm to over 6000 nm at 40 K. With using the filter bench, the DCR_{sys} of an MMF-coupled 9-pixel SNSPD array with an active area of 50 μm in diameter is greatly suppressed by 23 dB with 1 dB loss of system detection efficiency (SDE). The detector demonstrates an SDE of 51% at a DCR_{sys} of 100 Hz for 1550 nm photons. Thus, SNR of the detector is enhanced by about 160 times and the noise equivalent power is improved to 3×10^{-19} W/Hz$^{1/2}$.

Index Terms:

1. Introduction

As a high-performance single-photon detection technology [1], [2], superconducting nanowire single-photon detectors (SNSPDs) have played a key role in numerous applications, including

long-distance quantum key distribution [3], quantum optics [4], [5], and fluorescent observation [6]. Most of these applications use single-mode-fiber (SMF)-coupled SNSPDs, which have a typical active area of 20 μm or less in diameter.

System dark count rate (DCR_{sys}) is one of the key parameters of SNSPDs for practical applications. Generally, DCR_{sys} consists of intrinsic DCR (iDCR) and extrinsic DCR (eDCR). The iDCR exponentially increases with the bias current (I_b), which is related to the current-assisted motion of the vortex–antivortex pair [7], [8]. Usually, iDCR is negligible with a slightly low I_b. The eDCR is dominant in the low I_b region, which is contributed by the room-temperature blackbody radiation photons of the coupling fiber itself and the stray photons that penetrate into the fiber. For the SMF-coupled SNSPD, coiling SMF at low temperature can filter radiation photons over 2 μm, which is a straightforward way to reduce the DCR_{sys} [9]. Narrow bandpass filters (BPF) integrated on SNSPD chip [10] or on the SMF end face [11] were also developed to significantly reduce DCR_{sys} with a minimum insertion loss. Inserting bulky cryogenic optical filters at low temperature is another simple way to reduce the DCR_{sys}. Previously, Shibata *et al.* [12] introduced an SMF-to-SMF filter bench. In the experiment, a commercial BPF with a bandwidth of 10 nm and a block wavelength range of 400–1800 nm was applied, and DCR_{sys} was suppressed by approximately 29 dB with a 2.4-dB sacrifice in system detection efficiency (SDE $<$2%).

Free-space applications in the photon-starved regime, such as deep-space laser communication [13], [14], light detection and ranging [15]–[17], demand of either free-space-coupled or multimode-fiber (MMF)-coupled single-photon detectors with high SDE and low DCR_{sys} to improve their overall system performance [18]. Compared with SMF, MMF possesses a large numerical aperture (NA) and core diameter that can provide distinct advantages, such as high light-gathering capacity, low coupling loss, and easy alignment in free space to fiber coupling. Commercial infrared semiconductors, i.e., InGaAs avalanche photodiodes (APDs) with large active areas of over 50 μm in diameter, have been widely used. However, they are generally featured with a low SDE of less than 20% at 1550 nm and suffered from after-pulsing and high DCR_{sys} of approximately several kHz [19]–[21]. The reported MMF-coupled SNSPDs operated at an infrared wavelength 1550 nm also demonstrate a large DCR_{sys} over kHz [6], [22], which is mainly attributed to the broadband transmission of the blackbody radiation generated by the MMF at room temperature [23]. To date, few studies have been conducted to reduce the DCR_{sys} of MMF-coupled SNSPDs.

In this study, we designed a versatile packaged MMF-to-MMF filter bench to reduce the DCR_{sys} of MMF-coupled infrared SNSPD and improve its signal-to-noise ratio (SNR), which is often proportional to the ratio of SDE/DCR_{sys} [18], [3]. Through commercial and customized optical filters, the filter bench provides a high transmittance of approximately 80% at the central wavelength of the passband (1550 $\pm$ 12.5 nm) and a wide blocking range from 500 nm to over 6000 nm at 40 K. The DCR_{sys} of the MMF coupled 50-μm 9-pixel SNSPD array is reduced by approximately 23 dB (from 20 kHz to 100 Hz) using the filter bench, together with only 1 dB loss in SDE (from 64% to 51%). Thus, the SNR of the detector is improved by about 160 times and noise equivalent power (NEP) of the detector is improved from 3.9×10^{-18} W/Hz$^{1/2}$ to 3×10^{-19} W/Hz$^{1/2}$.

2. SNSPD Design and Characterization

A double-cavity structure 24, 25 was adopted to enhance the optical absorptance of nanowires, as shown in Fig. 1(a). A double-side thermally oxidized Si wafer was used as the substrate. The thickness of the oxide layer (SiO_2) is 268 nm (a quarter of 1550 nm) to enhance the transmittance of the photons. The NbN nanowire is embedded between two dielectric materials (SiO and SiO_2), and a 100-nm-thick gold mirror was stacked on top. The SDE of SNSPD is usually polarization-dependent, however, the polarization in MMF is difficult to control. To maximize the absorptance of the un-polarized 1550-nm photons, the thickness of the SiO layers was chose to be 160 nm, according to the simulation through COMSOL's Multiphysics software, In the simulation, a 6.5-nm thick and 80-nm wide NbN nanowire with 160-nm pitch was used. The simulated absorptance for this optimal case (160 nm SiO) is shown in Fig. 1(b). The absorptance for parallel ($A_{//}$) and

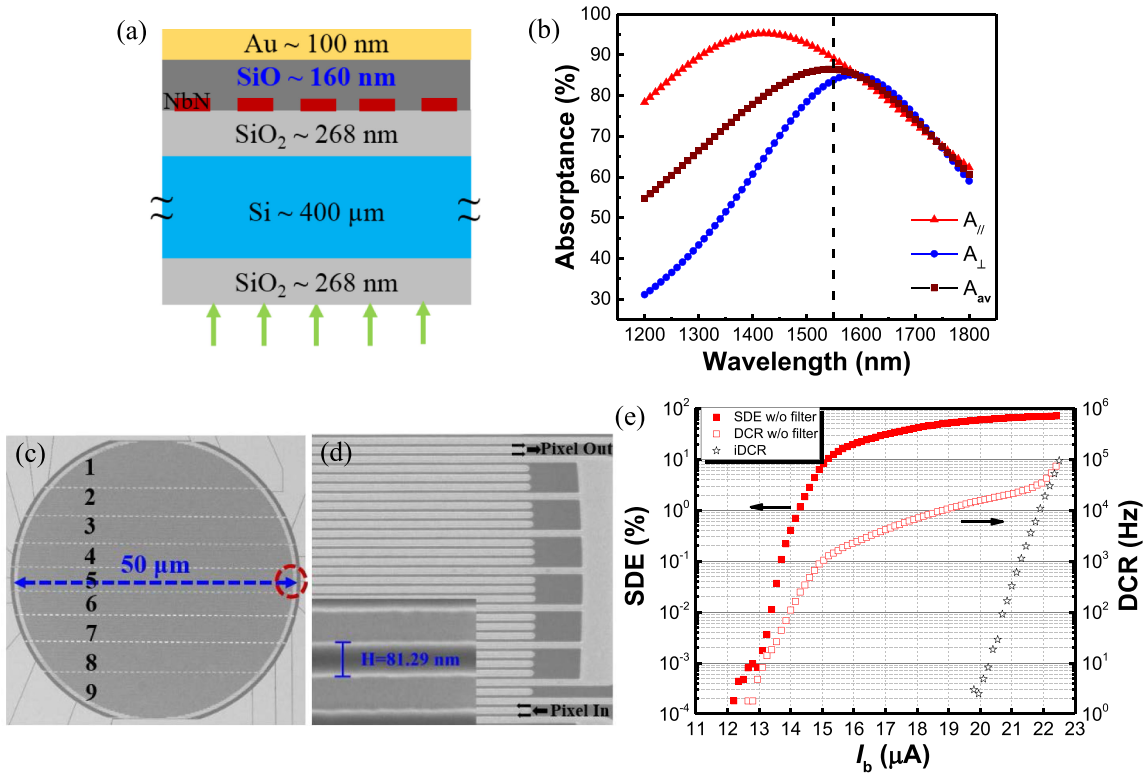

Fig. 1. (a) Schematic of optical structures used for SNSPD. Green arrows indicate incident detection of light, which is backside illumination. (b) Calculated optical absorptance at 1550 nm with optimized SiO thickness of 160 nm for a 6.5-nm-thick NbN nanowire with 80-nm width and 160-nm pitch. (c) SEM image of 9-pixel SNSPD array with 50-μm circular active area. (d) Magnified SEM image of middle pixel marked by red dashed circle in Fig. (c), showing the 2-SNAP structure in the pixel. Black arrows indicate the current flow direction. Inset shows a single nanowire with width of approximately 81 nm. (e) Total SDE and DCR of SNSPD without filter and iDCR as a function of I_b.

perpendicular ($A_{¥}$) polarized photons are 89% and 84%, respectively. Averaged absorptance at 1550 nm defined as $A_{av} = (A_{//} + A_{¥})/2$ is over 85%.

The active area of the SNSPD was designed to be 50 μm in diameter. To reduce the kinetic inductance (L_k) contributed by the long nanowire 26, the active area of the detector was divided into nine pixels. In addition, each pixel consisted of serially connected two superconducting nanowire avalanche photodetectors (SC-2SNAP) 27. Then, the devices were fabricated using a standard fabrication process 28. Fig. 1(c) shows a scanning electron microscopy (SEM) image of the 50-μm circular active area and 9 pixels. Fig. 1(d) presents a magnified SEM image of the area marked by the red dashed circle in Fig. 1(c), exhibiting the SC-2SNAP structure. The inset of Fig. 1(d) shows a zoom-in SEM photo of a 81 nm wide nanowire.

A lens MMF with a core diameter of 50 μm was aligned to the SNSPD to guide the 1550-nm photons, and the minimal focused beam size is approximately 30 μm in diameter 29, which is small enough to effectively coupling to the active area of the detector. The device was packaged and cooled in a 2.2-K Gifford–McMahon cryocooler. A tunable continuous wave 1550-nm laser (Keysight, 81940A) was used as light source. The input light was strongly attenuated to single-photon level (1×10^6 photons per second) by two cascaded attenuators. In the experiment, the SNSPD array was biased and read out by nine homemade electrical modules, the amplified output signals were fed to a multichannel counter. SDE and DCR_{sys} were both obtained from the output of the counter. DCR_{sys} was measured when the input 50-μm MMF was connected to the attenuator and the signal photons were blocked by shutter. iDCR was obtained when the device chip was placed in a 2.2-K shielded package block without a coupling fiber.

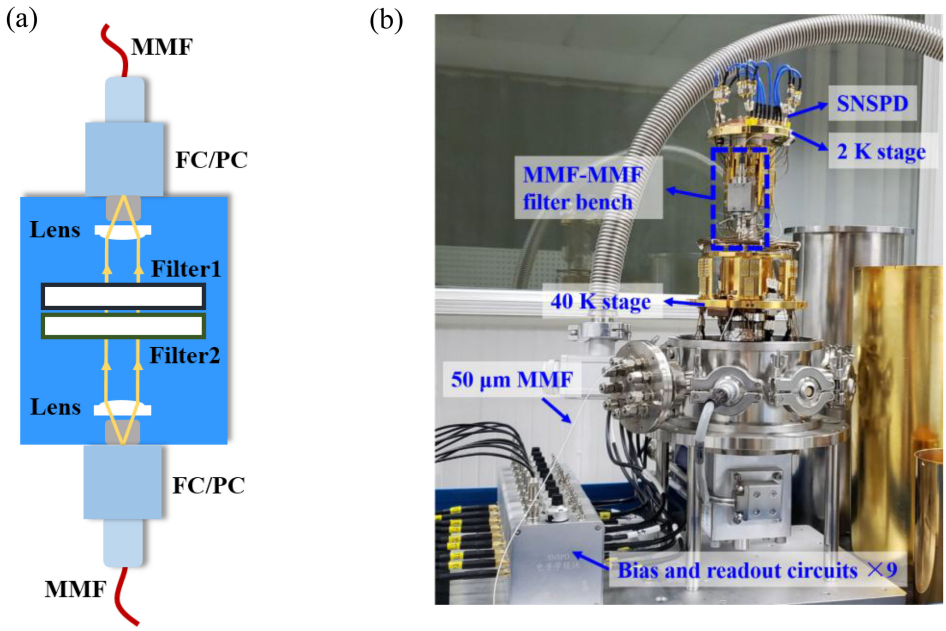

Fig. 2. (a) Schematic of fiber bench (not to scale). (b) Photograph of SNSPD cryostat mounted on an MMF-to-MMF filter bench on a 40 K stage, indicated by a dashed rectangle. The room-temperature readout circuits are also shown in the figure, as indicated by the labels.

SDE of the 9-pixel SNSPD array measured at different I_b is shown in Fig. 1(e). SDE is 71% at DCR_{sys} of 30 kHz. The iDCR data are indicated in Fig. 1(e) by black stars. DCR_{sys} is much higher than iDCR at low I_b region, e.g., the eDCR plays a major role when $I_b < 20.5\ \mu A$ ($0.9I_{sw}$, I_{sw} is the switching current). The large DCR_{sys} of the MMF-coupled SNSPD impairs its advantage over InGaAs avalanche photodiodes.

3. Suppressing DCR Using Cold Optical Filters

Owing to its large core diameter and wide transmission wavelength range, MMF placed at 300 K radiates a considerable amount of infrared photons ranging from approximately 2 μm to more than 10 μm [23]. These broadband thermal photons would propagate to the SNSPD through the fiber and trigger the detector with a certain probability. Unlike SMF, coiling fiber to filter the background photons is challenging for MMF due to the existence of multiple propagation modes. A reliable cryogenic optical filter with narrow passband, wide blocking range, and low insertion loss is versatile to effectively reduce the DCR_{sys} of the MMF-coupled SNSPD while maintaining a high SDE.

Unfortunately, manufacturing a single BPF that offers a wide blocking range from hundreds of nanometers to several microns and a narrow passband at 1550 nm is difficult. Inspired by Shibata *et al.* [12], we designed an MMF-to-MMF filter bench that consists of lenses and detachable optical filters. This bench allows us to use multiple optical filters to reduce the fabrication complexity of filters. Owing to the large NA and the large core diameter of MMF, the insertion loss of the bench without filters was about 0.45 (0.41) dB for 1550-nm wavelength measured at 40 K (room temperature), which is contributed by the interface loss of the collimated and focused lenses inside the bench and the misalignment of the parts.

Figure 2(a) shows a schematic design of the filter bench. The signal photons and room-temperature blackbody radiation photons propagate through the MMF then enter the free space inside the filter bench. After being filtered by the optical filters, the photons are coupled to the MMF on the opposite side of the bench via lenses and then propagate to the detector. The bench is made of invar steel, which has a small thermal expansion coefficient, thereby reducing the mechanical

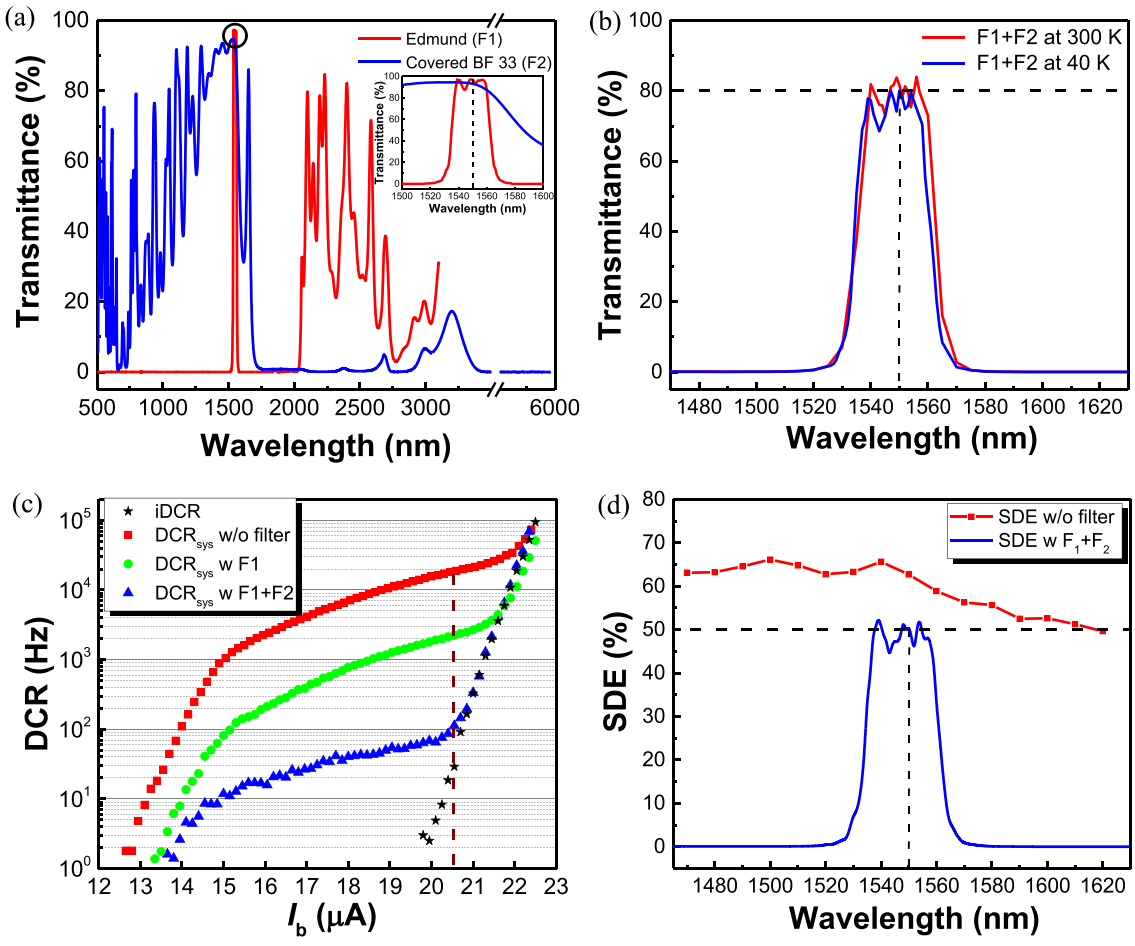

Fig. 3. (a) Transmission spectra measured at room temperature for a commercial BPF (F1, #87822, Edmund) and coated BF 33 glass. Inset of Fig. 3(a) shows details of photon transmittance ranging from 1500 nm to 1600 nm. (b) Transmittance of the filter bench with F1 + F2 measured at room temperature and 40 K, showing a blue shift of approximately 2 nm. (c) DCR_{sys} as a function of I_b, recorded under different conditions and illustrated by the label. (d) Wavelength dependence of SDE with and without F1 + F2, measured at $I_b = 0.9I_{sw}$.

deformation at low temperature. Fig. 2(b) shows a photo of our cryogenic system setup. The filter bench is attached to the 40-K stage, indicated by a dashed rectangle.

In this study, a commercial 1550-nm BPF (F1, #87822, Edmund) and a customized low-pass filter (F2) were used. The transmission spectra of F1 and F2 at room temperature are indicated in Fig. 3(a) by red and blue curves, respectively. The transmittance of F1 is 96% at 1550 nm and the bandwidth is 25 nm. The measured blocking range is from 500 to 2000 nm. The transmittance of F2, which was made of Borofloat 33 glass with 5 mm thickness, was approximately 95% at 1550 nm, and its blocking range is from 1600 nm to over 6000 nm. F1 and F2 were both mounted inside the bench. The total transmittance at 1550 nm of the bench with F1 + F2 at room temperature and at 40 K were measured to be 81.6% and 80%, respectively, as shown in Fig. 3(b). The small variation of the transmittance at the two different temperatures indicates a reliable optical coupling at the low temperature. A slight blue shift (approximately 2 nm) in the transmittance as a function of the wavelength can be explained by the weak temperature dependence of the refractive index of the dielectric materials of the filters.

Figure 3(c) shows the DCR of the SNSPD as a function of I_b measured at different filter conditions: without filter (red squares), with F1 (green dots), with F1 + F2 (blue triangles), and iDCR (black stars). We found that at $I_b = 0.9I_{sw}$, DCR_{sys} with F1 is about 4 kHz, which has a suppression of

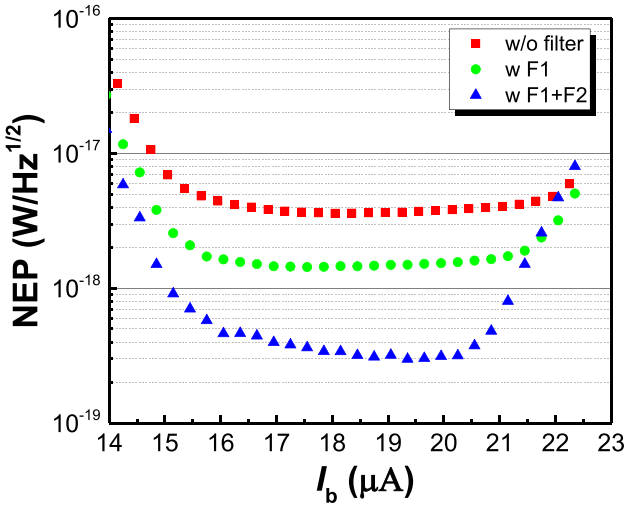

Fig. 4. Comparison of NEP without filter, with BPF F1, and with combined BPF F1and F2.

7 dB compared with the DCR_{sys} without filter (20 kHz). When F1 + F2 is used, DCR_{sys} is reduced to about 100 Hz, which has an impressive improvement of 23 dB.

Low suppression of SDE is also very important for the filter bench to obtain high SNR. Fig. 3(d) shows the wavelength dependence of the SDE with and without F1 + F2 at $I_b = 0.9I_{sw}$. The SDE without F1 + F2 decreases slightly with the increase of the wavelength due to unsaturated internal efficiency of the nanowire. The shape of SDE as a function of the wavelength with F1 + F2 indicated an evident BPF feature, with an averaged SDE of approximately 50% at the passband. As a result, the SDE with F1 + F2 at 1550 nm wavelength is suppressed by only 1 dB (from 64% to 51%), which is consistent with the measured transmittance. Therefore, we obtained a 50-μm MMF-coupled 9-pixel SNSPD array with SDE of 51% when the DCR_{sys} is 100 Hz, at which the SNR of our detector was improved about 160 times compared with the value without a filter bench. When F1 was replaced with a 10-nm bandwidth BPF (F3, #86088, Edmund), the DCR_{sys} was further reduced to 70 Hz at a bias of $0.9I_{sw}$, while the measured SDE is about 48.5% due to the lower transmittance of F3 at 1550 nm (approximately 85%).

Another common metric known as NEP $= h\nu\sqrt{2DCR_{sys}}$/SDE 30 was used to quantitatively evaluate the performance of the detector, where $h\nu$ is the photon energy. As shown in Fig. 4, the calculated NEP without a filter bench was approximately 3.9×10^{-18} W/Hz$^{1/2}$ at $0.9I_{sw}$, which was improved to 3.0×10^{-19} W/Hz$^{1/2}$ when both F1 and F2 were adopted.

Finally, the count rate (CR) and the timing jitter (T_j) of the detector were also characterized. The CR of the detector reaches 25 MHz with SDE of approximately 30%, owing to the 9-pixel and SC-2SNAP design. T_j was measured using a time-correlated single-photon counting module with resolution of 813 fs (SPC-150 board card, Becker & Hickl GmbH) 31. The photon source was a 1550-nm pulsed laser (FPL-01CAF, Calmar) with a pulse width of 100 fs, and the input photons were strongly attenuated to the single-photon level. The T_j of a single pixel, which is defined as the full width at half maximum of the Gaussian distribution, was approximately 60 ps at a bias of $0.9I_{sw}$. The total T_j of this detector was approximately 150 ps and was measured by combining the nine channel signals through a power combiner 28.

4. Discussion

Compared with the SMF bench, the MMF bench is more valuable because it has a lower insertion loss due to the large core diameter and the large NA. The SNR or NEP of our detector is much improved, in detail, the current SNR is about 50 times higher than semiconductor APDs [17]. In

future, several modifications can still be implemented to further improve the performance of the MMF-coupled SNSPD. Frist of all, there is still some room to reduce the active area of SNSPD, since the focused beam size of the lens MMF has a diameter of only 30 μm. A smaller active area of SNSPD will give both a higher maximum CR and probably a higher SDE. Secondly, an optimized filter set with a narrower bandwidth with a higher transmittance and a wider blocking range with a lower transmittance can further enhance the SNR.

5. Conclusion

To reduce the DCR_{sys} of the MMF-coupled SNSPD, we designed and characterized a cryogenic MMF-to-MMF filter bench. The filter bench demonstrated a wide block range from 500 nm to 6000 nm and narrow passband at 1550 $\pm$ 12.5 nm. By using the filter bench, DCR_{sys} was greatly suppressed by 23 dB with only 1 dB loss of SDE. SNR of the detector is improved by about 160 times and the NEP of the detector is improved from 3.9×10^{-18} W/Hz$^{1/2}$ to 3×10^{-19} W/Hz$^{1/2}$. The MMF-coupled 9-pixel SNSPD array with an active area of 50 μm in diameter showed an SDE of 51% at the DCR_{sys} of 100 Hz. The CR of the detector reaches 25 MHz with SDE of approximately 30%. This filter bench is versatile for MMFs with different core diameters and filters designed for various target wavelengths, which makes it a useful module for improving the SNR performance of the MMF-coupled SNSPDs in various applications.

References

[1] F. Marsili *et al.*, "Detecting single infrared photons with 93% system efficiency," *Nature Photon.*, vol. 7, pp. 210–214, 2013.

[2] W. J. Zhang *et al.*, "NbN superconducting nanowire single photon detector with efficiency over 90% at 1550 nm wavelength operational at compact cryocooler temperature," *Sci. China Phys. Mech. Astron.*, vol. 60, 2017, Art. no. 120314.

[3] H. L. Yin *et al.*, "Measurement-device-independent quantum key distribution over a 404 km optical fiber," *Phys. Rev. Lett.*, vol. 117, 2016, Art. no. 190501.

[4] R. H. Hadfield *et al.*, "Single photon source characterization with a superconducting single photon detector," *Opt. Exp.*, vol. 13, pp. 10846–10853, 2005.

[5] S. Dong *et al.*, "Energy-time entanglement generation in optical fibers under CW pumping," *Opt. Exp.*, vol. 22, pp. 359–368, 2014.

[6] T. Yamashita *et al.*, "Fluorescence correlation spectroscopy with visible-wavelength superconducting nanowire single-photon detector," *Opt. Exp.*, vol. 22, pp. 28783–28789, 2014.

[7] A. Eftekharian, H. Atikian, M. K. Akhlaghi, A. Jafari Salim, and A. Hamed Majedi, "Quantum ground state effect on fluctuation rates in nano-patterned superconducting structures," *Appl. Phys. Lett.*, vol. 103, 2013, Art. no. 242601.

[8] T. Yamashita *et al.*, "Origin of intrinsic dark count in superconducting nanowire single-photon detectors," *Appl. Phys. Lett.*, vol. 99, 2011, Art. no. 161105.

[9] K. Smirnov, Y. Vachtomin, A. Divochiy, A. Antipov, and G. Goltsman, "Dependence of dark count rates in superconducting single photon detectors on the filtering effect of standard single mode optical fibers," *Appl. Phys. Exp.*, vol. 8, 2015, Art. no. 022501.

[10] X. Yang *et al.*, "Superconducting nanowire single photon detector with on-chip bandpass filter," *Opt. Exp.*, vol. 22, pp. 16267–16272, 2014.

[11] W. J. Zhang *et al.*, "Fiber-coupled superconducting nanowire single-photon detectors integrated with a bandpass filter on the fiber end-face," *Supercond. Sci. Technol.*, vol. 31, 2018, Art. no. 035012.

[12] H. Shibata, K. Fukao, N. Kirigane, S. Karimoto, and H. Yamamoto, "SNSPD with ultimate low system dark count rate using various cold filters," *IEEE Trans. Appl. Supercond.*, vol. 27, no. 4, Jun. 2017, Art. no. 2200504.

[13] B. Fahs, M. Romanowicz, and M. M. Hella, "A Gbps building-to-building VLC link using standard CMOS avalanche photodiodes," *IEEE Photon. J.*, vol. 9, no. 6, Dec. 2017, Art. no. 7907709.

[14] H. M. Oubei, C. P. Li, K. H. Park, T. K. Ng, M. S. Alouini, and B. S. Ooi, "2.3 Gbit/s underwater wireless optical communications using directly modulated 520 nm laser diode," *Opt. Exp.*, vol. 23, pp. 20743–20748, 2015

[15] Z. J. Zhang, Y. Zhao, Y. Zhang, L. Wu, and J. Z. Su, "A real-time noise filtering strategy for photon counting 3D imaging lidar," *Opt. Exp.*, vol. 21, pp. 9247–9254, 2013.

[16] A. S. Huntington, G. M. Williams, and A. O. Lee, "Modeling false alarm rate and related characteristics of laser ranging and LIDAR avalanche photodiode photoreceivers," *Opt. Eng.*, vol. 57, 2018, Art. no. 073106.

[17] C. Yu, M. J. Shangguan, H. Y. Xia, J. Zhang, X. K. Dou, and J. W. Pan, "Fully integrated free-running InGaAs/InP single-photon detector for accurate lidar applications," *Opt. Exp.*, vol. 25, pp. 14611–14620, 2017.

[18] M. J. Shangguan *et al.*, "Dual-frequency Doppler lidar for wind detection with a superconducting nanowire single-photon detector," *Opt. Lett.*, vol. 42, pp. 3541–3544, 2017.

[19] A. R. Dixon, Z. L. Yuan, J. F. Dynes, A. W. Sharpe, and A. J. Shields, "Gigahertz decoy quantum key distribution with 1 Mbit/s secure key rate," *Opt. Exp.*, vol. 16, pp. 18790–18797, 2008.

[20] G. Wu, C. Y. Zhou, X. L. Chen, and H. P. Zeng, "High performance of gated-mode single-photon detector at 1.55 μm," *Opt. Commun.*, vol. 265, pp. 126–131, 2006.
[21] P. A. Hiskett *et al.*, "Performance and design of InGaAs/InP photodiodes for single-photon counting at 1.55 μm," *Appl. Opt.*, vol. 39, pp. 6818–6829, 2000.
[22] D. K. Liu, S. Miki, T. Yamashita, L. X. You, Z. Wang, and H. Terai, "Multimode fiber-coupled superconducting nanowire single-photon detector with 70% system efficiency at visible wavelength," *Opt. Exp.*, vol. 22, pp. 21167–21174, 2014.
[23] H. Shibata, K. Shimizu, H. Takesue, and Y. Tokura, "Superconducting nanowire single-photon detector with ultralow dark count rate using cold optical filters," *Appl. Phys. Exp.*, vol. 6, 2013, Art. no. 072801.
[24] D. Rosenberg, A. J. Kerman, R. J. Molnar, and E. A. Dauler, "High-speed and high-efficiency superconducting nanowire single photon detector array," *Opt. Exp.*, vol. 21, pp. 1440–1447, 2013.
[25] Y. Lixing *et al.*, "Superconducting nanowire single-photon detector on dielectric optical films for visible and near infrared wavelengths," *Supercond. Sci. Technol.*, vol. 30, 2017, Art. no. 084008.
[26] N. Calandri, Q. Y. Zhao, D. Zhu, A. Dane, and K. K. Berggren, "Superconducting nanowire detector jitter limited by detector geometry," *Appl. Phys. Lett.*, vol. 109, 2016, Art. no. 152601.
[27] S. Miki, M. Yabuno, T. Yamashita, and H. Terai, "Stable, high-performance operation of a fiber-coupled superconducting nanowire avalanche photon detector," *Opt. Exp.*, vol. 25, pp. 6796–6804, 2017.
[28] J. Huang *et al.*, "High speed superconducting nanowire single-photon detector with nine interleaved nanowires," *Supercond. Sci. Technol.*, vol. 31, 2018, Art. no. 074001.
[29] H. Li *et al.*, "Large-sensitive-area superconducting nanowire single-photon detector at 850 nm with high detection efficiency," *Opt. Exp.*, vol. 23, pp. 17301–17308, 2015.
[30] G. N. Gol'tsman *et al.*, "Ultrafast superconducting single-photon detectors for near-infrared-wavelength quantum communications," *Physica Status Solidi C—Conf. Crit. Rev.*, vol. 2, no. 5, pp. 1480–1488, 2005.
[31] L. X. You *et al.*, "Jitter analysis of a superconducting nanowire single photon detector," *AIP Adv.*, vol. 3, 2013, Art. no. 072135.